

Localized Andreev edge states in HgTe quantum wells

I. M. Khaymovich,^{1,2} N. M. Chtchelkatchev,^{2,3,4,5} and V. M. Vinokur²

¹*Institute for Physics of Microstructures, Russian Academy of Sciences, 603950 Nizhny Novgorod, GSP-105, Russia*

²*Argonne National Laboratory, Argonne, IL 60439, USA*

³*Institute for High Pressure Physics, Russian Academy of Sciences, Troitsk 142190, Moscow Region, Russia*

⁴*L. D. Landau Institute for Theoretical Physics, Russian Academy of Sciences, 117940 Moscow, Russia*

⁵*Department of Theoretical Physics, Moscow Institute of Physics and Technology, 141700 Moscow, Russia*

(Dated: November 23, 2018)

We investigate the interplay of superconductivity and the topological order in the topological insulator (TI) formed in HgTe-CdTe quantum wells coupled to the s -wave isotropic superconductor (SC) placed on top of CdTe layer. Proximity effect induces superconducting correlations in TI effecting classification of the TI electronic states. Depending on the strength of the coupling and the initial chemical potentials in SC and TI, the edge states either (i) become gapped, or (ii) hybridize into localized Andreev states, or else (iii) merge with the bulk states turning the TI into an anisotropic narrow-gap semiconductor.

A topological insulator (TI), a material in which the electronic spectrum possesses an energy gap in the bulk but has special, so-called topologically protected, edge (surface) states falling into this gap, is one of the focal points of current condensed matter studies. TI have the potential for utilization in integrated circuits due to ability of the topologically protected edge states to carry nearly dissipationless current, and the question how robust the edge states may be with respect to hybridization with the spectrum of the leads has become a focal point of much research. In this Letter we investigate the effect of superconducting correlations on topologically protected edge states in TI comprised of the quantum wells (QW) of mercury telluride (HgTe) sandwiched between the cadmium telluride (CdTe) banks [1–4] brought into a contact with the SC layer, see Fig. 1. We find, in particular, that while “topologically protected” edge states can ensure undisturbed propagation of the charge (spin) carriers, superconducting correlations can block the edge current causing a peculiar localization effect.

In the absence of superconducting correlations the edge states spectrum is linear near the Fermi surface, comprising of two counter-propagating electron and two hole branches, respectively [2]. Importantly, the edge spectrum is isotropic in a sense that it does not depend on the orientation of the edges with respect to crystallographic axes, although the edge electronic states wave functions are orientation dependent. Namely, there is a phase difference between the wave function components corresponding to (E) or (H)-subbands in TI. The bulk spectrum is characterized by the gap M . At small SC-TI coupling (the quantitative criteria will be given below) the edge-states spectrum acquire a gap E_g . Furthermore, superconducting correlations mix the subband branches and thus turn the resulting electronic spectrum in TI (edge and bulk), anisotropic, and E_g starts to depend on orientation of the edge. This can cause localization of the low-lying edge states since an inevitable bending of the edge will create the regions along the edge where the

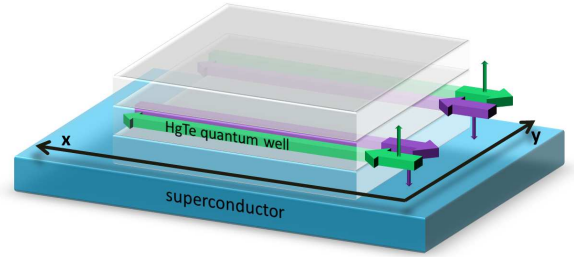


FIG. 1. (Color online) Sketch of the 2D topological insulator coupled to a superconductor. The thick arrows show schematically the edge states.

edge-particle energy $\varepsilon < E_g$ thus getting locked between the turning points where $\varepsilon = E_g$. At the turning points electron and hole excitations undergo Andreev reflection and form the localized Andreev bound edge states, see Fig. 2a. As the characteristic energy of the induced pairing amplitude exceeds M then the gap of the continuum bulk states of TI collapses and TI behaves like the highly anisotropic narrow-gap semiconductor.

The low energy Hamiltonian of the two-dimensional (2D) topological insulator formed in the HgTe QW has the form, see e.g. the review Ref. [2]:

$$\tilde{\mathcal{H}} = \begin{pmatrix} \hat{H} & 0 \\ 0 & \hat{H} \end{pmatrix}, \quad (1)$$

where $\hat{H} = \epsilon_k + d_i \hat{\sigma}^i$, $i = \{1, 2, 3\}$; $\hat{\sigma}^i$ are the Pauli matrices acting in the subband (isospin) space; $\epsilon_k = C - Dk^2$. We choose the frame of reference so that $\vec{d} = (k_x A, -k_y A, M - Bk^2)$. Here A, B, C, D and M are material parameters. The lower block of the Hamiltonian, $\hat{H} = \hat{\rho}^T \tilde{\mathcal{H}}^* \hat{\rho} = \epsilon_k - d_i (-k) \hat{\sigma}^i$, where $\hat{\rho} = i\hat{\sigma}_y$ is the metric tensor in the spinor space. The chosen representation for $\tilde{\mathcal{H}}$ enables us to employ the machinery of the tensor bispinor algebra developed for Dirac Hamiltonian.

To construct the convenient form of the Bogoliubov –

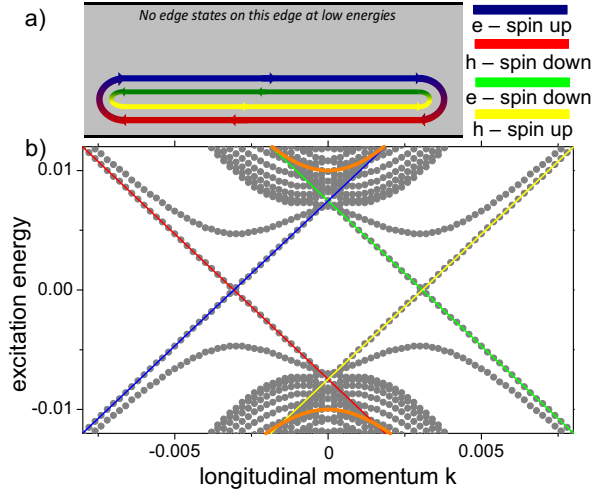


FIG. 2. (Color online) a) Electronic states in TI coupled to a superconductor. a) A sketch of localized Andreev edge states in TI. b) Excitation spectrum in the 2D TI with proximity effect induced superconducting correlations: the edge modes at one TI-edge acquired the gap while the edge modes on the opposite edge remain gapless. Solid lines show the edge states and bulk spectrum boundaries in TI without superconducting correlations. Here k_0 is the edge state crossing momentum. The parameters are chosen as: $mk_F/(2\pi\hbar^2)t_a^2/M = 1$, $t_b = \sqrt{|B_-|/|B_+|}t_a$ and the orientation angle $\varphi = 0$.

de Gennes (BdG) Hamiltonian describing superconductivity, we introduce first the time reversal symmetry operator as

$$\tilde{\mathcal{T}} = \begin{pmatrix} 0 & 0 & 0 & -1 \\ 0 & 0 & 1 & 0 \\ 0 & -1 & 0 & 0 \\ 1 & 0 & 0 & 0 \end{pmatrix} \mathcal{C} = -\hat{\tau}_1 \otimes i\hat{\sigma}_2 \mathcal{C}, \quad (2)$$

where \mathcal{C} is the operator of the complex conjugation and $\hat{\tau}_i$, are the Pauli matrices acting in spin space. Then the time-reverse of the BHZ-Hamiltonian (1) is $\tilde{\mathcal{T}}\tilde{\mathcal{H}}\tilde{\mathcal{T}}^{-1} = \tilde{\mathcal{H}}$. The BdG Hamiltonian is

$$\mathcal{H}_{\text{BDG}} = \begin{pmatrix} \tilde{\mathcal{H}} + \tilde{\mathcal{U}} & \tilde{\Delta}_{\text{TI}} \\ \tilde{\Delta}_{\text{TI}}^\dagger & -\tilde{\mathcal{H}} - \tilde{\mathcal{T}}\tilde{\mathcal{U}}\tilde{\mathcal{T}}^{-1} \end{pmatrix}, \quad (3)$$

where $\tilde{\Delta}_{\text{TI}}$ is the effective proximity induced superconducting pairing matrix coupling the spin and subband spaces. The effective chemical potential shift appearing in the BCS theory has matrix form $\tilde{\mathcal{U}}$; both, $\tilde{\Delta}_{\text{TI}}$ and $\tilde{\mathcal{U}}$ will be found below microscopically.

To proceed further we present the Hamiltonian describing the TI-SC coupling in a form:

$$H = H_{sc} + H_{2D} + H_{\text{int}}. \quad (4)$$

The superconducting part is

$$H_{sc} = \sum_{s=\uparrow,\downarrow} \int d^3r \Psi_s^\dagger(\mathbf{r}) (\epsilon_{sc} - \mu) \Psi_s(\mathbf{r}) + \int d^3r \left(\Delta \Psi_\uparrow^\dagger(\mathbf{r}) \Psi_\downarrow^\dagger(\mathbf{r}) + \Delta^* \Psi_\downarrow(\mathbf{r}) \Psi_\uparrow(\mathbf{r}) \right) \quad (5)$$

where, $\Psi_{\uparrow(\downarrow)}$ ($\Psi_{\uparrow(\downarrow)}^\dagger$) are the field annihilation (creation) operators for the state with the spin up (down) in the coordinate representation, Δ is the superconducting gap, ϵ_{sc} is the single electron kinetic energy, and μ is the Fermi energy.

The second quantization representation for the TI Hamiltonian is written in the basis of the Wannier functions for particles with spin s :

$$H_{2D,s} = \sum_{\mathbf{R}\mathbf{R}',s} \sum_{\sigma,\sigma'=a,b} c_{s\mathbf{R},\sigma}^\dagger (\epsilon_{2D,s}(\mathbf{R}\sigma, \mathbf{R}'\sigma') + C\delta(\mathbf{R}, \mathbf{R}')\delta_{\sigma,\sigma''}) c_{s\mathbf{R}',\sigma'} \quad (6)$$

where $\epsilon_{2D,s}(\mathbf{R}, \mathbf{R}')$ is the lattice representation of the BHZ-model (1) (see [6]). Then $H_{2D} = \sum_s H_{2D,s}$.

Finally, H_{int} reflects the electronic tunnelling between the SC and TI:

$$H_{\text{int}} = \sum_{\mathbf{R},s} \sum_{\sigma=a,b} \left(t_{\sigma,\mathbf{R}} \Psi_s^\dagger(\mathbf{R}) c_{s\mathbf{R},\sigma} + t_{\sigma,\mathbf{R}}^* c_{s\mathbf{R},\sigma}^\dagger \Psi_s(\mathbf{R}) \right),$$

where $c_{\uparrow(\downarrow)\mathbf{R},a}$ is the superposition of $|\Gamma_6, \pm\frac{1}{2}\rangle$, $|\Gamma_8, \pm\frac{1}{2}\rangle$ and $c_{\uparrow(\downarrow)\mathbf{R},b}$ refers to the subband $|\Gamma_6, \pm\frac{3}{2}\rangle$. Integrating out the bulk superconductor variables $\Psi_s(\mathbf{R})$ one obtains the effective BdG-Hamiltonian (3) for the homogeneous tunneling amplitudes $t_{\sigma\mathbf{R}} = t_\sigma$, with the matrix superconducting order parameter and the effective chemical potential shift having the form:

$$\tilde{\Delta}_{\text{TI}} = \begin{pmatrix} \hat{\Delta}_{\text{TI}} & 0 \\ 0 & \hat{\Delta}_{\text{TI}} \end{pmatrix}, \quad \tilde{\mathcal{U}} = \begin{pmatrix} \hat{\mathcal{U}} & 0 \\ 0 & \hat{\mathcal{U}} \end{pmatrix}. \quad (7)$$

Here

$$\hat{\Delta}_{\text{TI}} = -\frac{mk_F}{2\pi\hbar^2} \begin{pmatrix} t_a^{*2} & t_a^* t_b^* \\ t_a^* t_b^* & t_b^{*2} \end{pmatrix}, \quad \hat{\Delta}_{\text{TI}} = \hat{\rho}^T \hat{\Delta}_{\text{TI}} \hat{\rho}, \quad (8)$$

$$\hat{\mathcal{U}} = \frac{m}{2\pi\hbar^2 a_{\text{TI}}} \begin{pmatrix} |t_a|^2 & t_a^* t_b \\ t_a t_b^* & |t_b|^2 \end{pmatrix}, \quad \hat{\mathcal{U}} = \hat{\rho}^T \hat{\mathcal{U}} \hat{\rho}, \quad (9)$$

m and k_F are the effective mass and the Fermi momentum of the bulk superconductor respectively, a_{TI} is the characteristic length scale of the order of the lattice constant in TI. Since $\Delta_{\text{TI}} \ll \Delta$, the proximity induced parameters are independent of Δ [5].

For numerical calculations we take typical parameters: $A = 3.8$ eVÅ, $B = -56.2$ eVÅ², $D = -38.7$ eVÅ². Without a loss of generality we take the energy-shift parameter $C = 0$. We do not fix M ($-10\text{meV} \lesssim M < 0$) and use it as the energy unit. Our numerical and analytical calculations show the approximate

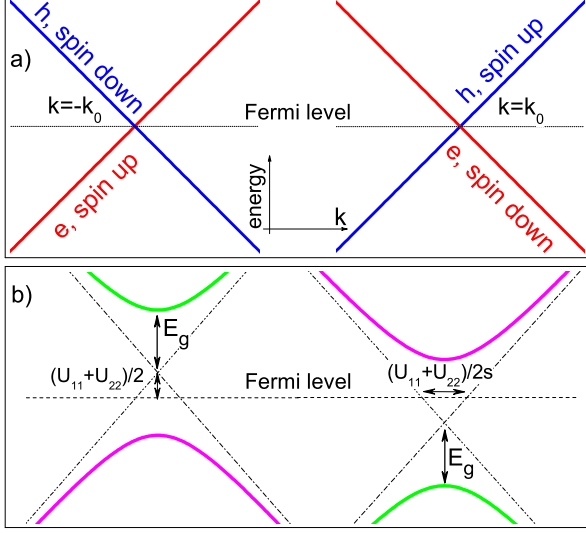


FIG. 3. (Color online) The edge states at the TI boundary for a weak coupling where the edge states become gapped. a) Unperturbed edge-spectrum. b) Edge states with the proximity-induced gap. The shift of the zero point reflects the difference in the original chemical potentials.

symmetry relation that satisfies the spectrum of \mathcal{H}_{BDG} : $\chi E(\mathbf{k}/\chi, M/\chi, t_a/\sqrt{\chi}, t_b/\sqrt{\chi}) \approx E(\mathbf{k}, M, t_a, t_b)$, where χ is a dimensionless scaling parameter. The scaling relation appears since M is much smaller than the energy scales one can construct from A , B and D . In addition, M appears to be the most sensitive to the HgTe layer width: it changes with it by several orders of magnitude while the other parameters change by $\sim 20\%$ and their changes very slightly modify the spectrum [2].

First we discuss “weak” superconductivity where superconducting correlations induced in TI can be treated perturbatively. In this case matrix elements of $\tilde{\Delta}_{\text{TI}}$ and $\tilde{\mathcal{U}}$ are smaller than the gap in the continuum spectrum, M , in the bulk of TI. In the absence of superconducting correlations $\tilde{\Delta}_{\text{TI}} = 0$ and $\tilde{\mathcal{U}} = 0$, and there are two electron and two hole edge states at each TI surface. The edge states have the linear dispersion law with the velocity $s = A|\sqrt{B_+B_-}/B|$, where $B_{\pm} = B \pm D$. They cross the Fermi energy at $k = k_0 = DM/(A\sqrt{B_+B_-})$ and $k = -k_0$, see Fig. 3a. We denote the wave functions of the electron and hole edge states near $k = k_0$ as $\psi^{(1)} = (\psi_{\text{edge}}, \hat{0}, \hat{0}, \hat{0})^T$ and $\psi^{(2)} = (\hat{0}, \hat{0}, \psi_{\text{edge}}, \hat{0})^T$, respectively, where $\hat{0}$ is the zero spinor in the subband space,

$$\psi_{\text{edge}} = \frac{e^{-i\hat{\sigma}_z\varphi/2}}{\sqrt{2|B|}} \begin{pmatrix} \sqrt{|B_-|} \\ -\sqrt{|B_+|} \end{pmatrix} \times (e^{-\lambda_+ \mathbf{r} \cdot \mathbf{n}} - e^{-\lambda_- \mathbf{r} \cdot \mathbf{n}}) e^{ik\mathbf{r} \cdot \mathbf{l}}, \quad (10)$$

k is the momentum component parallel to the edge, $\mathbf{r} = (x, y)$, \mathbf{l} , and \mathbf{n} are the unit vectors directed along the TI boundary and perpendicular to it correspondingly $[\mathbf{l} \times \mathbf{n}$

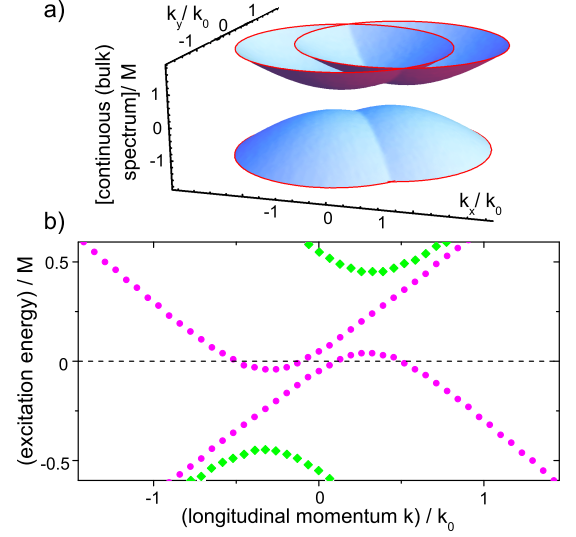


FIG. 4. (Color online) Bulk and edge states for the intermediate coupling. a) Energy of the bulk states as function of k_x, k_y . Without superconductivity, the bulk states dispersion is isotropic, $E(k) = \epsilon(k) \pm \sqrt{A^2k^2 + (M - Bk^2)^2}$ [2], where $k = \sqrt{k_x^2 + k_y^2}$. Superconducting correlations make it anisotropic as follows from the noncommutativity of $\tilde{\Delta}$ and/or $\tilde{\mathcal{U}}$ with \mathcal{H} in Eq.(3). b) Gapped edges states. The colors for the families of the dispersion curves are the same as in Fig. 3. The parameters are chosen as: $mk_F/(2\pi\hbar^2)t_a^2/M = 1$, $t_b = \sqrt{|B_-|/|B_+|}t_a \exp(i\pi/6)$ and the orientation angle $\varphi = \pi/2$.

is aligned with the OZ axis], and φ is the angle between \mathbf{l} and OX axis. The decay length scales of the edge states into the bulk of the topological insulators are:

$$\lambda_{\pm} = \lambda_0 \pm \sqrt{\left(k - \frac{D}{B}\lambda_0\right)^2 + \frac{A^2}{4B^2} - \frac{M}{B}}, \quad (11)$$

where $\lambda_0 = A/(2\sqrt{B_+B_-})$. We stress that spinor components of ψ_{edge} depend on the orientation of the TI boundary.

The dispersion law of the edge states near $k = k_0$ within the framework of the perturbation theory taking in the account the superconducting correlations acquires the form:

$$\epsilon_{1,2}(k) = (\mathcal{U}_{11} + \mathcal{U}_{22} \pm \omega(k))/2, \quad (12)$$

where $\omega = \sqrt{(2s(k - k_0) + \mathcal{U}_{11} - \mathcal{U}_{22})^2 + 4E_g^2}$; \mathcal{U}_{ii} , $i = 1, 2$ are the matrix elements of $\tilde{\mathcal{U}}$ with respect to the states $\psi^{(1,2)}$ and $E_g = |(\tilde{\Delta}_{\text{TI}})_{12}|$. They can be parameterized through $\mathcal{T}_{\pm} = [t_a\sqrt{|B_-|} - t_b\sqrt{|B_+|}e^{\pm i\varphi}]$. So,

$$E_g = \mathcal{T}_+ \mathcal{T}_-, \quad (13)$$

while $\tilde{\mathcal{U}}_{11} = \alpha\mathcal{T}_+^2$ and $\tilde{\mathcal{U}}_{22} = -\alpha\mathcal{T}_-^2$, where $\alpha = (k_F a_{\text{TI}})^{-1}$, see Eq.(9).

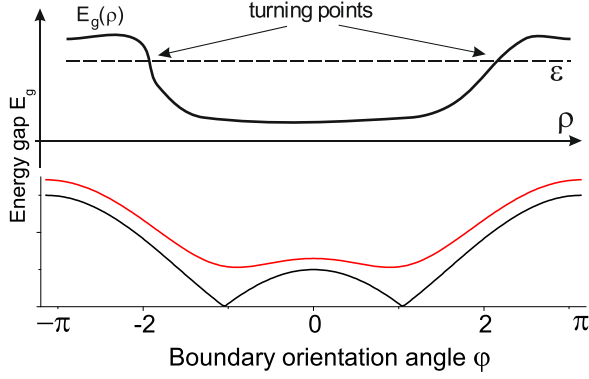


FIG. 5. (Color online) Energy landscape for the edge states. a) Sketch of the energy landscape along the edge (parametrized by the coordinate ρ). The magnitude of the gap may change as a result of spatial fluctuations (like change in a shape of the TI boundary or fluctuations in tunneling amplitudes) and the state with the energy ϵ would appear trapped between the turning points where $\epsilon < E_g$ forming Andreev bound edge state like it is shown in Fig. 2. b) Calculated E_g as function of the edge orientation angle φ for the ratio $t_a/t_b \sqrt{|B_-/B_+|} \exp(-i\pi/3)$ equal to 1 (upper curve) and 2 (bottom curve).

What happens with the edge state energy levels when E_g is finite is illustrated in Fig. 3-4. However, the level splitting is not a general situation. It is possible that E_g is very small or even equal to zero when $\mathcal{T}_+ = 0$ or $\mathcal{T}_- = 0$. A particular picture depends on the edge orientation angle φ and/or on the tunneling amplitudes, t_a and t_b . Shown in the Fig. 2 is the situation where at one boundary of the TI-strip the edge states remain gapless ($E_g = 0$) while at the opposite boundary $E_g \neq 0$ and the edge states have the gap. The strip in Fig. 2 is not infinite, there are points at the edge where the TI-boundary changes its direction and, at the same time, the value of E_g changes. At these “turning points” electron and hole edge (going in the opposite direction) with the energy smaller than new E_g undergo Andreev reflection and form the Andreev bound edge state, see Figs. 2,5. To implement this situation the TI sample can be shaped into a disc for which the dependence of the gap upon the orientation angle φ of the edge, can be easily computed, see Fig. 5b.

Now we discuss a general nonperturbative situation. The excitation spectrum in 2D TI accounting for the proximity induced superconducting correlations in the case where proximity induced potentials in TI are of the same order as the gap in TI without superconductor on top is shown in Fig. 6. The gap between the branches of the continuum spectrum nearly closes and TI acquires effectively metallic conductivity with the relativistic spectrum similar to that in graphene. Solid lines correspond to the edge states and bulk spectrum boundaries in TI without superconducting correlations.

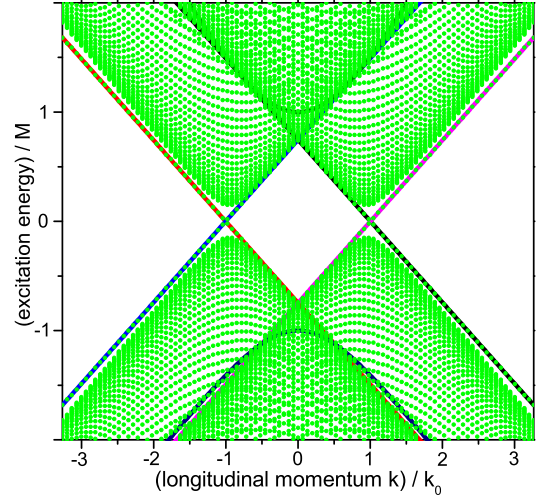


FIG. 6. Excitation spectrum in 2D TI for the proximity induced potentials being of the same order as the gap in TI in the absence of a SC. The gap between the branches of the continuum spectrum collapses and TI acquires metallic conductivity with the relativistic spectrum similar to that in graphene. Solid lines correspond to the edge states and the bulk spectrum boundaries in TI without superconducting correlations. Parameters are chosen as: $mkF/(2\pi\hbar^2)t_a^2/M = 12$, $\varphi = 0$, and $t_b = \sqrt{|B_-|/|B_+|}t_a$.

To conclude, we investigated topologically protected edge states in quantum wells (QW) of HgTe sandwiched between CdTe and demonstrated that the s -wave isotropic superconductor placed on top of CdTe layer induces superconducting correlations in the TI revealing the built in anisotropy of TI which did not affect the spectrum when superconducting correlations were absent. The form of the edge states spectrum essentially depends on the edge orientation with respect to crystallographic directions of the TI. Depending on the coupling between the superconductor and 2D TI, different scenarios can be realized: (i) the edge states of the topological insulator acquire a gap, (ii) the edge states hybridize into the Andreev localized edge state and/or (iii) the gap separating the continuum and the edge modes collapses and TI becomes the narrowgap (anisotropic) semiconductor. Our predictions can be verified by means of, for example, scanning tunnelling spectroscopy measurements of the spectra showed in Fig. 3 where the shift of the zero point $U_{11} + U_{22}$ can be tuned by the gate placed on top of the CdTe layer.

This work was supported by the U.S. Department of Energy Office of Science under the Contract No. DE-AC02-06CH11357, the work of IMK and NMC was partly supported by the Russian president foundation (mk-7674.2010.2) under the Federal program “Scientific and educational personnel of innovative Russia”.

[6] Details are given in the supplementary material.

-
- [1] B. A. Volkov and O. A. Pankratov, JETP Lett. **42**, 142 (1985).
 [2] X. Qi and S-C. Zhang, arXiv:1008.2026v1.
 [3] B. A. Bernevig, *et al.*, Science **314**, 1757 (2006).
 [4] M. König, *et al.*, Science **318**, 766 (2007).
 [5] A. S. Mel'nikov, N. B. Kopnin (unpublished).
-

Supplementary material

Lattice model

Microscopic description of the coupling between TI and the superconductor developed on the base of the standard lattice regularization of the BHZ-model (1) replacing its parameters by [2]:

$$\epsilon_k = C - 2Da^{-2} [2 - \cos k_x a - \cos k_y a], \quad (14)$$

$$\vec{d} = (Aa^{-1} \sin k_x a, -Aa^{-1} \sin k_y a, M - Ba^{-2} [2 - \cos k_x a - \cos k_y a]). \quad (15)$$

This corresponds to the quadratic Bravais lattice (with the translation vectors $\mathbf{a}_1 = ax_0$, $\mathbf{a}_2 = ay_0$) with two type of states (corresponding annihilation operators are $\hat{c}_{a\mathbf{R}}$ and $\hat{c}_{b\mathbf{R}}$) on each site replying to subband states. Therefore the Hamiltonian describing TI in the second quantization representation in the basis of the Wannier functions for particles with spin s , takes the form:

$$\hat{H}_{2D,s} = \sum_{\mathbf{R}\mathbf{R}',s} \sum_{\sigma,\sigma'=a,b} \hat{c}_{s\mathbf{R},\sigma}^+ (\hat{\epsilon}_{2D,s}(\mathbf{R}\sigma, \mathbf{R}'\sigma') + C\delta(\mathbf{R}, \mathbf{R}')\delta_{\sigma,\sigma'}) \hat{c}_{s\mathbf{R}',\sigma'} \quad (16)$$

where

$$\hat{\epsilon}_{2D,s}(\mathbf{R}\tilde{\sigma}, \mathbf{R}'\tilde{\sigma}) = \delta_{\mathbf{R}\mathbf{R}'} \left[\left(M - \frac{4B}{a^2} \right) \tilde{\sigma} - \frac{4D}{a^2} \right] + \left(\frac{4B}{a^2} \tilde{\sigma} + \frac{4D}{a^2} \right) (\delta_{\mathbf{R}+\mathbf{a}_1, \mathbf{R}'} + \delta_{\mathbf{R}-\mathbf{a}_1, \mathbf{R}'} + \delta_{\mathbf{R}+\mathbf{a}_2, \mathbf{R}'} + \delta_{\mathbf{R}-\mathbf{a}_2, \mathbf{R}'} \quad (17a)$$

$$\hat{\epsilon}_{2D,\uparrow}(\mathbf{R}a, \mathbf{R}'b) = -\hat{\epsilon}_{2D,\downarrow}(\mathbf{R}b, \mathbf{R}'a) = \frac{A}{2a} (\delta_{\mathbf{R}+\mathbf{a}_2, \mathbf{R}'} - \delta_{\mathbf{R}-\mathbf{a}_2, \mathbf{R}'} - i\delta_{\mathbf{R}+\mathbf{a}_1, \mathbf{R}'} + i\delta_{\mathbf{R}-\mathbf{a}_1, \mathbf{R}'} \quad (17b)$$

$$\hat{\epsilon}_{2D,\uparrow}(\mathbf{R}b, \mathbf{R}'a) = -\hat{\epsilon}_{2D,\downarrow}(\mathbf{R}a, \mathbf{R}'b) = -\hat{\epsilon}_{2D,\uparrow}^*(\mathbf{R}a, \mathbf{R}'b). \quad (17c)$$
